β-Molybdenum nitride: synthesis mechanism and catalytic response in the gas phase hydrogenation of p-chloronitrobenzene

Cárdenas-Lizana, F.; Gómez-Quero, S.; Perret, N.; Kiwi-Minsker, L.; Keane, M.A.

DOI
10.1039/c0cy00011f

Publication date
2011

Document Version
Final published version

Published in
Catalysis Science & Technology

Catalysis
Science & Technology

Cite this: *Catal. Sci. Technol.*, 2011, **1**, 794–801

www.rsc.org/catalysis

PAPER

β-Molybdenum nitride: synthesis mechanism and catalytic response in the gas phase hydrogenation of *p*-chloronitrobenzene

Fernando Cárdenas-Lizana,*[a] Santiago Gómez-Quero,[b] Noémie Perret,[c] Lioubov Kiwi-Minsker[a] and Mark A. Keane*[c]

Received 8th October 2010, Accepted 14th December 2010
DOI: 10.1039/c0cy00011f

A temperature programmed treatment of MoO_3 in flowing $N_2 + H_2$ has been employed to prepare β-phase molybdenum nitride (β-Mo_2N) which has been used to promote, for the first time, the catalytic hydrogenation of *p*-chloronitrobenzene. The reduction/nitridation synthesis steps have been monitored *in situ* and the starting oxide, reaction intermediates and nitride product have been identified and characterized by powder X-ray diffraction (XRD), diffuse reflectance UV-Vis (DRS UV-Vis), elemental analysis, scanning electron microscopy (SEM) and BET/pore volume measurements. Our results demonstrate that $MoO_3 \rightarrow$ β-Mo_2N is a kinetically controlled process where an initial reduction stage generates (sequentially) MoO_2 and Mo as reaction intermediates with a subsequent incorporation of N to produce β-Mo_2N. SEM analysis has established that the transformation is non-topotactic with a disruption to the platelet morphology that characterizes MoO_3 and an increase in BET area (from 1 $m^2\ g^{-1}$ to 17 $m^2\ g^{-1}$). Moreover, temperature programmed desorption measurements have revealed a significant hydrogen uptake (0.71 μmol m^{-2}) on β-Mo_2N. This has been exploited in the hydrogenation of *p*-chloronitrobenzene where *p*-chloroaniline was generated as the sole product with an associated rate constant ($k = 2.0\ min^{-1}$) that is higher than values recorded for supported transition metals. Our study establishes the reaction mechanism involved in the synthesis of β-Mo_2N and demonstrates its viability to promote selective $-NO_2$ group reduction as an alternative sustainable, high throughput route to commercially important haloamines.

1. Introduction

Transition-metal nitrides in general, and Mo nitride in particular, exhibit a combination of properties that have resulted in multiple applications as coatings/structural components,[1] high performance magnets,[2] in electronic and optical devices[3] and as catalytic materials.[4,5] Conventional preparative routes have involved either (a) high temperature (1400–1900 K) reaction of the base metal and elemental nitrogen,[6] (b) carbothermal nitridation of metal oxides[6] or (c) a self-propagating high temperature synthesis.[7] Alternative methods that can operate under milder reaction conditions have drawn on controlled temperature programmed procedures. Examples include the reaction of MoO_3 with NH_3[8–11] and $N_2 + H_2$,[12,13] reaction of $MoCl_5$ with urea,[14] reduction of MoO_2 with NH_4Cl,[15] chemical vapour deposition of $MoCl_5$ (in the presence of NH_3)[16] and the thermal decomposition of $(HMT)_2(NH_4)_4Mo_7O_{24}$.[17,18] A combination of $NH_3 + H_2$ has been the most widely employed reacting gas in reduction–nitridation processes.[4,19,20] However, the use of a $N_2 + H_2$ mixture circumvents the heat transfer problems associated with the endothermic NH_3 decomposition.[12] The methodologies applied to date have generated a combination of Mo_xN_y phases, principally metastable cubic (γ-Mo_2N) and hexagonal (δ-MoN) structures.[6] Although γ-Mo_2N is the most commonly synthesized form by thermal treatment of MoO_3,[9,12,19,21] there is also evidence in the literature for the formation of a body centred tetragonal β-nitride phase with a Mo/N ratio in the range 2.0–2.6.[13,22–26]

The literature dealing with the temperature programmed synthesis of Mo nitrides is still quite limited and we could not find any comprehensive analysis of the mechanism(s) involved in the formation of β-Mo nitride from MoO_3. It is, however, worth noting a number of reports that deal (in part) with Mo nitride preparation,[13,23,24,27–29] physical/chemical properties[6] and morphology.[13,24] We can also flag published studies in which the formation of partially reduced oxides (Mo_4O_{11},[30] MoO_2)[9] or ordered bronzes (H_xMoO_3, $0.07 < x < 0.34$)[31] and/or Mo[22] have been observed during the reduction–nitridation

[a] *Group of Catalytic Reaction Engineering, Ecole Polytechnique Fédérale de Lausanne (GGRC-ISIC-EPFL), Lausanne, Switzerland. E-mail: fernando.cardenaslizana@epfl.ch; Tel: +41 (0)21 693 31 86*
[b] *Van't Hoff Institute for Molecular Sciences, University of Amsterdam, The Netherlands*
[c] *Chemical Engineering, School of Engineering and Physical Sciences, Heriot-Watt University, Edinburgh EH14 4AS, Scotland, UK. E-mail: M.A.Keane@hw.ac.uk; Tel: +44 (0)131 4514719*

process. Nagai *et al.*[23] recorded the formation of MoO_2, γ-Mo_2N, β-Mo_2N and Mo during treatment of MoO_3 with NH_3 up to 1173 K. In terms of applications, it has been reported that group VI nitrides can exhibit comparable catalytic activity in hydrogen mediated reactions to that obtained with conventional metal catalysts.[4,32] This has been ascribed to a contraction of the d-band and modification of electron density due to the incorporation of N interstitially in the metal lattice,[33] resulting in a capacity for H_2 adsorption.[4] Molybdenum nitrides have been successfully used to promote the hydrogenation of long chain alkadienes,[34] CO[35] and ethylene,[36] the hydrodenitrogenation of carbazole[23,28,37] and the hydrodesulfuration of thiophene[13,24] and dibenzothiophene.[38] Moreover, Mckay *et al.*, in a recent study,[39] demonstrated an enhanced catalytic response in ammonia synthesis for β-Mo_2N (prepared by MoO_3 treatment in H_2/N_2 at 973 K) when compared with δ-MoN and γ-Mo_2N. However, we were unable to find any study in the open literature dealing with the hydrogenation of nitro-compounds over molybdenum nitride.

In this paper, we set out to explicitly identify the intermediates in β-Mo nitride synthesis and report the first application of this nitride in the catalytic hydrogenation of nitroarenes. The selective hydrogenation of *p*-chloronitrobenzene (*p*-CNB) to *p*-chloroaniline (*p*-CAN) has been selected as a model reaction. *p*-CAN is a high production volume compound,[40] extensively used in the manufacture of a range of fine chemicals.[41] Existing routes to *p*-CAN involve high pressure batch liquid phase operations that generate toxic by-products with a low overall yield[42] and there is now a pressing demand for alternative cleaner catalytic routes. In this study, we establish the feasibility of β-Mo nitride as a catalytic material to promote the continuous gas phase hydrogenation of *p*-CNB to *p*-CAN.

2. Results and discussion

2.1 β-Mo_2N synthesis and characterization

2.1.1 Synthesis mechanism

2.1.1.1 TPR. The commercial MoO_3 sample (as received), when subjected to a temperature programmed treatment in 15% v/v N_2/H_2 to 933 K, generated the profile presented in Fig. 1(A). The emergence of four positive (H_2 consumption) peaks suggests four separate reaction steps. To probe this response, the thermal treatment was repeated, stopping at different stages in order to generate eight samples for *ex situ* analysis, as identified in Fig. 1(A). Sample selection included starting material (1), final product (8) and intermediate samples (2–4 and 6) obtained pre- and post- a stage of significant H_2 consumption. Given the broadness of the two final peaks, samples 5 and 7 were taken at the peak maxima. Sample 2 was selected, although no significant response was noted, as there is some evidence in the literature[31] of a transition from MoO_3 to MoO_2 at this temperature (623 K). The associated time, temperature related peak maxima (T_{max}), BET surface area, total pore volume and phase composition associated with each sample are given in Table 1. Taking the profile in Fig. 1(A), intermediate(s) formation and conversion occurred during the final isothermal (933 K) hold, suggesting a kinetically

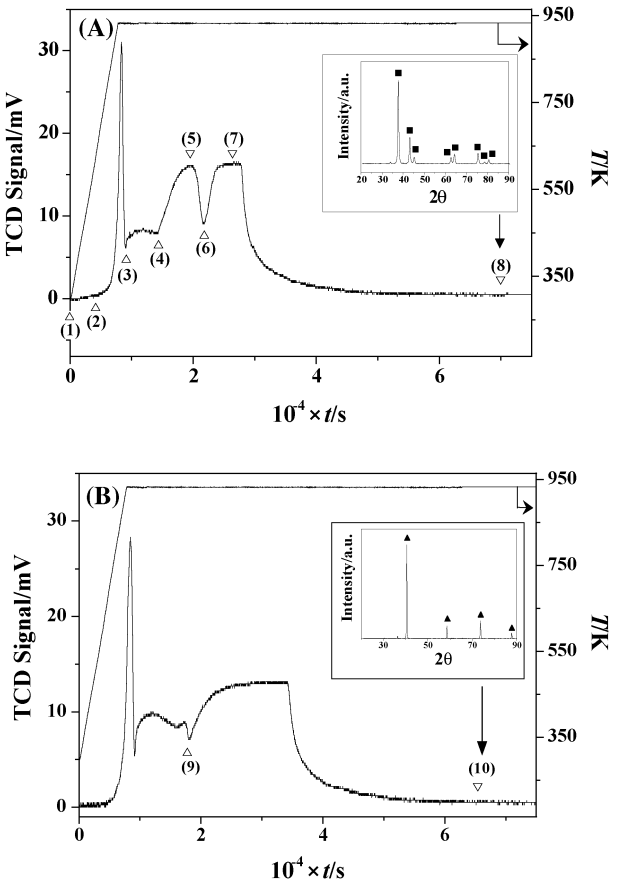

Fig. 1 TCD response resulting from the temperature programmed treatment of MoO_3 (at 5 K min^{-1} to 933 K) in (A) 15% v/v N_2/H_2 and (B) 15% v/v Ar/H_2. Insets: XRD patterns for the passivated products post thermal treatment. Note: peak assignments based on JCPDS-ICDD standards for (A) β-Mo_2N (25-1368, ■) and (B) Mo (42-1120, ▲).

controlled process. In contrast, previous studies have suggested that Mo nitride intermediate(s) formation was temperature dependant, *i.e.* thermochemically controlled: MoO_2 (613–773 K)[9,12,13,43]; H_xMoO_x (≤623 K)[31,43,44]; Mo_4O_{11} (673 K)[45]; γ-$Mo_2O_xN_{1-x}$ (773 K)[46]; Mo (900–1153 K).[13,45,47]

2.1.1.2 XRD/elemental analysis/DRS UV-Vis. Powder XRD patterns of passivated samples (see experimental section) obtained at points 1–8 are presented in Fig. 2. It has been established previously[48] that the passivation step provides a protective oxide surface layer without deeper oxidation. In order to confirm the composition of each sample, the XRD patterns were compared with commercial samples (MoO_3 (A), MoO_2 (B) and Mo (C)) and the JCPDS-ICDD standards for MoO_3 (35-0609), MoO_2 (32-0671), Mo (42-1120) and β-Mo_2N (25-1368, (D)). In Fig. 2, each of the four columns represent the specific contribution at that stage of reduction and/or nitridation (1–8) due to (A) MoO_3, (B) MoO_2, (C) Mo and (D) β-Mo_2N and serves to illustrate the evolution of the MoO_3 reactant to β-Mo_2N product. The diffractogram for the final product shows peaks at 37.73°, 43.14°, 45.28°, 62.67°, 64.28°, 75.48°, 78.64° and 80.54° (Fig. 2, profile 8-D), which are consistent with the (112), (200), (004), (220), (204), (312),

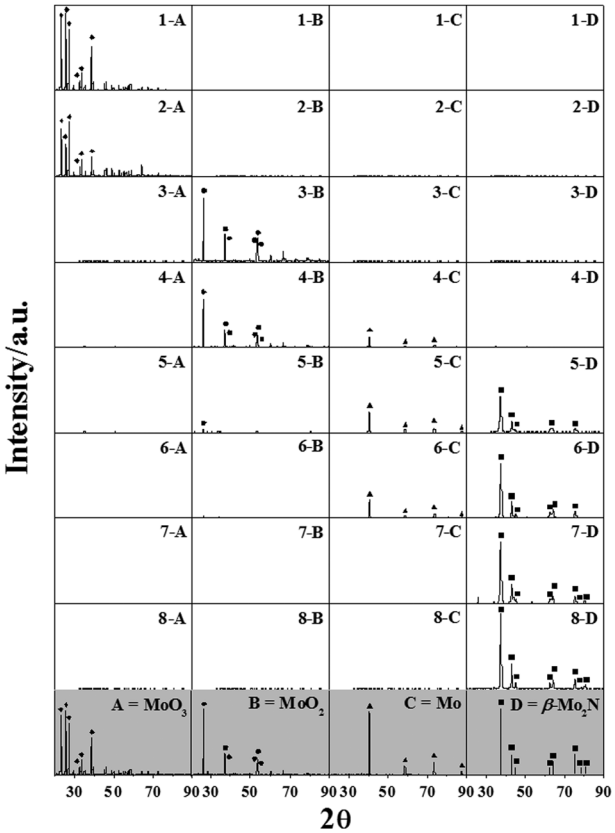

Fig. 2 XRD profiles of samples 1–8 (see Fig. 1(A)) focusing on the contributions due to (A) MoO_3, (B) MoO_2, (C) Mo and (D) β-Mo_2N. Diffractograms for model samples and peak assignment based on JCPDS-ICDD reference data are denoted by A (MoO_3; Alfa Aesar, 99.9995; 35-0609, ◆), B (MoO_2; Aldrich, 99%; 32-0671, ●), C (Mo; Aldrich, ≥ 99.9%; 42-1120, ▲) and D (JCPDS-ICDD β-Mo_2N standard (25-1368), ■).

(116) and (224) reflections of bulk β-Mo_2N. This result agrees with the findings of Gong *et al.*[13] who reported the formation of β-Mo_2N *via* temperature programmed treatment of MoO_3 with N_2 + H_2 at 923–1023 K. In contrast, Nagai and co-workers[23,28] proposed that β-phase formation (from MoO_3 treatment in NH_3) required a higher synthesis temperature where the conversion of the (cubic) γ-phase to the β-form occurred at 1070 K (in He). A decrease in the intensity of the characteristic signals for MoO_3 in Fig. 2 (comparing profiles 1-A with 2-A) suggests a transformation of the trioxide over the temperature range 298–623 K. While Ressler *et al.*[31] have proposed a transition of MoO_3 to MoO_2 at 623 K, we observed no detectable signals due to (bulk) MoO_2 associated with sample 2 (see profile 2-B). The sharp H_2 TPR consumption peak recorded at 933 K (between samples 2 and 3, see Fig. 1(A)) can be attributed to the reduction of MoO_3 to MoO_2 as confirmed in profile 3-B (Fig. 2). Moreover, the amount of H_2 associated with this signal matched that required for the oxide reduction (to within ±10%), confirming the sole transition of trioxide to Mo dioxide. Furthermore, the ill-defined positive peak between points 3 and 4 (Fig. 1(A)) can be linked to a partial reduction of MoO_2 to Mo (Fig. 2, profile 4-C and Table 1). The latter proceeds further from stage 4 to 5 (Fig. 1(A)) where the XRD response for sample 5 shows only trace MoO_2. Nitrogen consumption generated a negative TCD signal (see Fig. 1(A)) and the XRD profiles for samples 5 and 6 are consistent with the nitridation of Mo (profiles 5-D and 6-D in Fig. 2). The nitridation process is complete by stage 7, at which point there was no detectable Mo present (Fig. 2, Table 1). Moreover, elemental analysis of samples 5 and 7 revealed an increase in nitrogen content (from 2.4 ± 0.3 to 5.7 ± 0.3% w/w), which can be attributed to the progressive nitridation of Mo. Samples 7 and 8 exhibited equivalent nitrogen contents, close to that for β-Mo_2N. The occurrence of a final positive signal (stage 6–8, Fig. 1(A)) can be attributed to H_2 uptake on β-Mo_2N.[4] Our results confirm that the reaction of MoO_3 with N_2 + H_2 follows the sequence:

$$MoO_3 \xrightarrow[-H_2O]{+H_2} MoO_2 \xrightarrow[-H_2O]{+H_2} Mo \xrightarrow{+N_2} \beta\text{-}Mo_2N$$

Previous studies have suggested the participation of MoO_2,[9,10,12,13,24] MoO_xH_y,[31,43,44] Mo_4O_{11}[49,50] and Mo[13,24] as intermediates during the temperature programmed treatment of MoO_3 to form Mo nitride. Matsuda *et al.*[44] proposed the reduction pathway $MoO_3 \rightarrow H_xMoO_3 \rightarrow MoO_2$ for reaction at 623 K, Wise and Markel[12] suggested the steps $MoO_3 \rightarrow MoO_2 \rightarrow Mo$ at 773 K and Słoczyński[51] reported $MoO_3 \rightarrow Mo_4O_{11} \rightarrow MoO_2$ where $T < 823$ K. In order to facilitate identification of the reaction intermediates, DRS UV-Vis measurements were also conducted (see Fig. 3). Profiles 1 and 2 (representing samples 1 and 2, Fig. 1(A)) exhibit bands centred at 248 and 325 nm. We can draw on the literature[52] for MoO_3 where bands at 220–250 nm and 320 nm have been observed and attributed to tetrahedral Mo–O and octahedral Mo–O–Mo bridging, respectively. The appearance of the higher wavelength band (at 325 nm) in profile 2 suggests a partial transition of Mo^{6+} from tetrahedral to octahedral coordination, a result that is in line with findings reported by Aritani *et al.*[53] The broad band over the 400–600 nm range for

Table 1 Reaction time, temperature related TCD signal maximum (T_{max}), BET surface area, total pore volume and % fraction of each phase associated with the passivated samples: see Fig. 1(A)

Sample	Time/min	T_{max}/K	BET area/m^2 g^{-1}	Pore volume (10^{-3} cm^3 g^{-1})	% (Phase)
(1)	0	298	1	2	100 (MoO_3)
(2)	69	623	2	3	100 (MoO_3)
(3)	150	933	2	3	100 (MoO_2)
(4)	240	933	6	7	90 (MoO_2) 10 (Mo)
(5)	325	933	14	11	25 (Mo) 75 (β-Mo_2N)
(6)	365	933	14	10	20 (Mo) 80 (β-Mo_2N)
(7)	440	933	14	10	100 (β-Mo_2N)
(8)	1165	933	17	11	100 (β-Mo_2N)

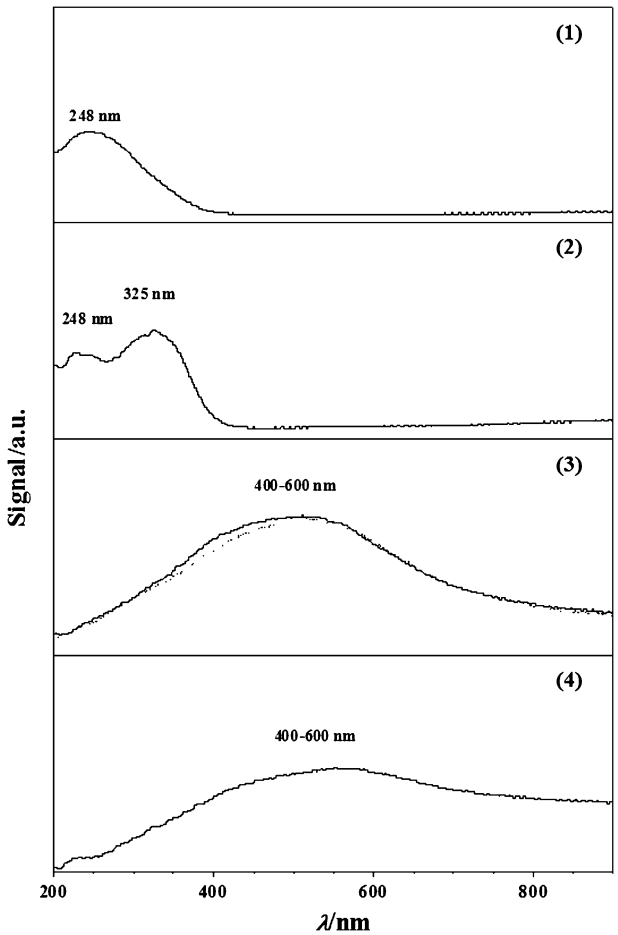

Fig. 3 DRS UV-Vis spectra of samples 1–4 (see Fig. 1(A)); dotted line in profile (3) represents spectrum for commercial MoO_2 (Aldrich, 99%).

samples 3 and 4 suggests the formation of Mo^{5+} and/or Mo^{4+} [54,55] and is consistent with our TPR (Fig. 1(A)) and XRD (Fig. 2) measurements, *i.e.* MoO_2 is produced at the final isothermal (933 K) hold (see Table 1). Indeed the UV-Vis spectrum associated with sample 3 coincides directly with that recorded for the commercial MoO_2 (dotted profile). The decrease in intensity of the MoO_2 signal for sample 4 (profile 4) can be attributed to a partial reduction to Mo during steps 3 and 4 (see Fig. 1(A) and 2).

2.1.1.3 Stepwise reduction/nitridation and denitridation. Our results for the solid transformation of MoO_3 in $N_2 + H_2$ to β-Mo_2N are consistent with the formation of MoO_2 and Mo as intermediates, *i.e.* a first stage that involves the conversion of MoO_3 to MoO_2 (sample 3 in Fig. 1(A)) with subsequent reduction to metallic Mo. Nitrogen is then incorporated into the solid in a nitridation step. In order to decouple the reduction and nitridation steps and further confirm this reaction mechanism, we monitored the temperature programmed treatment of MoO_3 in H_2 + Ar, *i.e.* in the absence of N_2, which delivered the profile shown in Fig. 1(B). The final product (at 933 K) in this instance was Mo as confirmed by XRD analysis (see the inset in Fig. 1(B)). By comparing the profile obtained for thermal treatment in $N_2 + H_2$ (Fig. 1(A)) with that in Ar + H_2 (Fig. 1(B)), any observed differences can be attributed to the involvement of nitridation step(s) in the former. In both cases, the patterns coincide up to the point at which MoO_2 is partially reduced (sample 4 in Fig. 1(A) and sample 9 in Fig. 1(B)), where the associated XRD patterns are consistent with a mixture of MoO_2 + Mo; see profiles 4-B and 4-C in Fig. 2 for thermal treatment in $N_2 + H_2$, equivalent to that obtained in Ar + H_2. Additional hydrogen consumption in the Ar + H_2 treatment, *i.e.* positive signal (samples 9 and 10 in Fig. 1(B)), can be attributed to H_2 uptake on Mo as has been reported elsewhere.[56,57] Further treatment of the Mo sample in $N_2 + H_2$ resulted in the sole formation of β-Mo_2N as confirmed by XRD analysis (diffractogram pattern not shown). We have also investigated the reversibility of the nitridation step by considering a thermally (to 1273 K) induced denitridation of sample 8 (see Fig. 1(A)). The resultant profile is shown in Fig. 4 where the amount of nitrogen released was consistent with the content in the starting sample. Nitride decomposition generated Mo as the sole product, which was confirmed by XRD analysis (see the inset in Fig. 4). This result finds support in the literature where the generation of Mo has been reported from γ-Mo_2N (*via* β-Mo_2N at 1073 K) for treatment (in He) at $T \geq 1153$.[23,47]

2.1.1.4 SEM/BET/pore volume. A solid to solid transition can be termed topotactic if the structural atomic arrangement is conserved in terms of the relative position of the metal atoms.[58] It has been shown that Mo nitrides can be synthesized by controlled thermal treatment of MoO_3 with NH_3 [8,33,59] or $N_2 + H_2$ [60] *via* a topotactic route, where a continuous transformation through oxynitride(s) takes place.[44] A non-topotactic formation of β-Mo_2N has also been proposed in the literature[22,24] but without any explicit evidence to support this. In order to consider the morphology and structural evolution of the solid during the preparation of β-Mo_2N, SEM analysis was conducted. The representative SEM images of the starting MoO_3, given in Fig. 5, clearly show a platelet orthorhombic crystal structure, as reported elsewhere.[6,61] SEM analysis of the β-Mo_2N product (sample 8 in Fig. 1(A)) indicates a

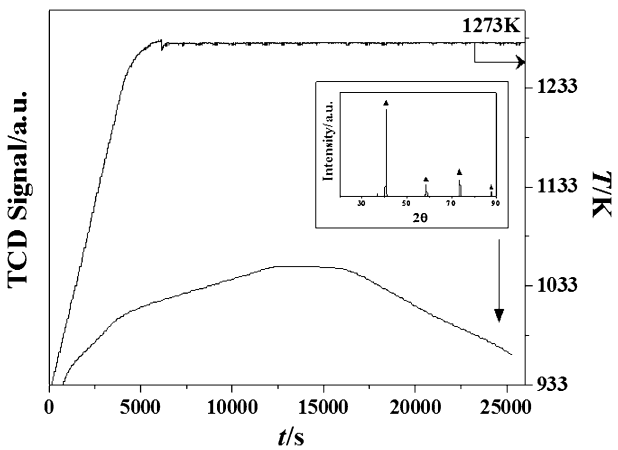

Fig. 4 TCD response for the temperature programmed treatment of β-Mo_2N to 1273 K (at 5 K min^{-1}) in He. Inset: XRD pattern for passivated product post thermal treatment. Note: peak assignments based on the JCPDS-ICDD standard for Mo (42-1120, ▲).

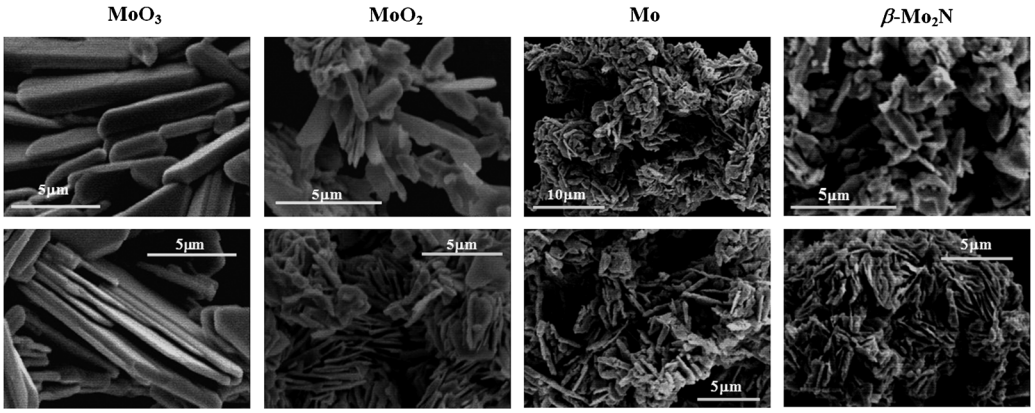

Fig. 5 SEM micrographs of starting MoO_3 (sample 1, Fig. 1(A); first row, Fig. 2), passivated MoO_2 (sample 3, Fig. 1(A); third row, Fig. 2), Mo (sample 10, Fig. 1(B)) and β-Mo_2N (sample 8, Fig. 1(A); eighth row, Fig. 2).

non-topotactic transformation, *i.e.* disruption of the platelet morphology during the reduction–nitridation process. Moreover, the SEM micrographs of MoO_2 (sample 3 in Fig. 1(A)) and Mo (sample 10 in Fig. 1(B)) reveal a morphology similar to that of β-Mo_2N, suggesting that the disruption of the crystal configuration takes place during the $MoO_3 \rightarrow MoO_2$ reduction step. We provide here the first demonstrable evidence for a non-topotactic transformation, identifying the critical step(s) and intermediate(s). The BET areas and total pore volume of the samples obtained during reduction/nitridation are given in Table 1. The starting MoO_3 (pale yellow crystalline powder) exhibited a negligible surface area (1 $m^2\ g^{-1}$) and low pore volume (2×10^{-3} $cm^3\ g^{-1}$). As reduction/nitridation proceeded, MoO_3 was transformed into a light gray (sample 2, Fig. 1(A)), gray (samples 3–6) and ultimately a lustrous gray-black solid (β-Mo_2N). An increase in both BET ($1 \rightarrow 17$ $m^2\ g^{-1}$) and pore volume ($2 \times 10^{-3} \rightarrow 11 \times 10^{-3}$ $cm^3\ g^{-1}$) was observed with the transformation of MoO_3 into β-Mo_2N. Nagai *et al.*[23] recorded a surface area of 18 $m^2\ g^{-1}$ for β-Mo_2N synthesised from MoO_3 (1 $m^2\ g^{-1}$) in a temperature controlled reduction–nitridation using NH_3 while Gong *et al.*[13] achieved BET areas in the range 2–9 $m^2\ g^{-1}$ with $N_2 + H_2$ under similar synthesis conditions. It should be noted that the most significant increase in surface area was associated with the reduction of MoO_2 to Mo (sample 3 to 4) and the subsequent nitridation to β-Mo_2N (sample 4 to 5). Schulmeyer and Ortner[62] reported that the conversion of MoO_2 (in H_2) to Mo was accompanied (on the basis of SEM analysis) by the formation of surface cracks and craters as a result of the stresses associated with oxygen removal, which can contribute to the higher BET value. We could not find any data on pore volume changes during β-Mo_2N synthesis: our analysis (Table 1) reveals an increase in the total pore volume that was accompanied by a greater surface area.

2.1.2 H_2-TPD. The possibility of hydrogen uptake by the nitride (Fig. 1(A), stage 6–7) has been confirmed by the H_2-TPD response recorded for sample 8 and is shown in Fig. 6; the degree of reproducibility can be assessed from the repeated measurements that are presented. The profile exhibits three different stages of hydrogen release at 412 K, 640 K and 803 K, which suggests different degrees of interaction of H_2 with β-Mo_2N. The ability of Mo nitrides to adsorb hydrogen has been noted in the review by Furimsky[4] where the reported studies have either focused on the γ-phase or did not specify the allotropic form. Guerrero-Ruiz *et al.*[63] demonstrated the co-existence of different surface sites for hydrogen adsorption on Mo_2N (with a BET area of 8 $m^2\ g^{-1}$). Li and co-workers[64] reported a dependence of hydrogen adsorption–desorption on the treatment temperature where at $T > 500$ K the presence of three distinct hydrogen species located on the surface, subsurface and bulk of Mo_2N was proposed and discussed in terms of a dissociation (on Mo–N) and diffusion mechanism. Nitrogen removal post-H_2 treatment has been reported in the literature[20,65] and associated with desorption peaks at $T > 823$ K.[66] In this study, the nitride structure was unaffected by the TPD treatment as can be evaluated from the XRD response pre- and post-TPD (see insets in Fig. 6); there was no significant change in nitrogen content post-TPD. The overall amount of H_2 released was 0.71 μmol m^{-2}, a value that is close to that reported (0.78 μmol m^{-2}) by Li *et al.*[67] for Mo_2N, although the authors did not identify the crystallographic phase.

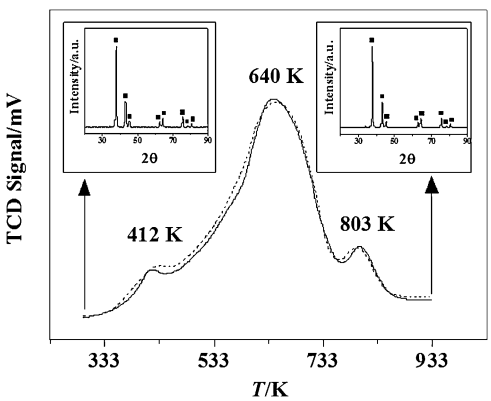

Fig. 6 Hydrogen TPD response for β-Mo_2N (50 K min^{-1} to 933 K) in Ar (dotted and solid lines represent two separate measurements). Insets: XRD patterns for samples pre- and post-TPD. Note: peak assignments based on the JCPDS-ICDD standard for β-Mo_2N (25-1368, ■).

2.2 Gas phase hydrogenation of *p*-chloronitrobenzene (*p*-CNB)

The observed capacity of β-Mo_2N for hydrogen uptake suggests possible hydrogenation properties. We tested this in the gas phase hydrogenation of *p*-CNB where *p*-CAN was detected as the sole product. There was no evidence of aromatic ring hydrogenation or hydrogenolysis of the –Cl or –NO_2 substituents. This ultra-selectivity with respect to –NO_2 group reduction is a significant result as the hydrogenation of *p*-CNB has been invariably accompanied by dechlorination and side-reactions resulting in the formation of azoxyderivates,[68,69] aniline[70–72] and nitrobenzene.[71–73] This has been a feature of reaction over Ru–Ir/γ-Al_2O_3,[68] silica supported group VIII metals (Ag, Cu, Co Fe and Ni),[69] $PtMO_x$ (M = Sm, Pr, Ce, Nd and La) supported on carbon nanotubes[71] and unsupported NiB alloys (as nanotubes (20–25 nm)[73] and nanoparticles (6–100 nm)).[70,72] The variation in fractional *p*-CNB conversion ($X_{p\text{-CNB}}$) as a function of time-on-stream is presented (as an inset) in Fig. 7. An initial temporal decline in conversion is in evidence with a subsequent steady state at extended reaction times (>250 min). The temporal variation of conversion can be expressed in terms of the empirical relationship[74]

$$\frac{(X_{p\text{-CNB}} - X_0)}{(X_{300\,\text{min}} - X_0)} = \frac{\Delta t}{(\beta + \Delta t)} \qquad (1)$$

where $X_{300\text{min}}$ represents fractional conversion after 300 min on-stream and β is a time scale fitting parameter. Fit convergence ($R^2 > 0.99$) yields values for X_0 (initial conversion). For reactor operation under plug-flow conditions where hydrogen was maintained far in excess, the following reactor/kinetic expression applies

$$\ln\left[\frac{1}{1 - X_0}\right] = k \times \left(\frac{n}{F}\right) \qquad (2)$$

where k (min^{-1}) is the pseudo-first order kinetic constant and n/F (min) has the physical meaning of contact time. The associated linear relationship (forced through the origin, see Fig. 7) serves to validate our approach and the resultant k = 2.0 min^{-1}. This value exceeds the rate constants (0.1–0.3 min^{-1}) that we have previously recorded (over the T range 453–523 K) for *p*-CNB → *p*-CAN promoted using Au/Al_2O_3[75,76] and Au/TiO_2.[76] Reaction over Pd/Al_2O_3 also

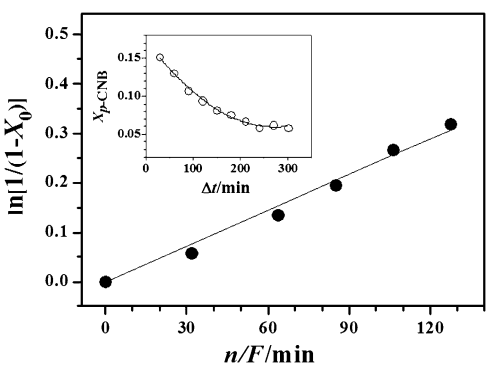

Fig. 7 Pseudo-first order kinetic plot for the hydrogenation of *p*-CNB over β-Mo_2N; line represents fit to eqn (2). Inset: variation of *p*-CNB fractional conversion ($X_{p\text{-CNB}}$) with time-on-stream; n/F = 85 min; line represents fit to eqn (1). T = 493 K.

delivered a lower rate (k = 1.5 min^{-1}),[75] albeit at a lower reaction temperature (453 K) but nitrobenzene and aniline were formed as the principal products. Moreover, catalytic nitroarene hydrogenation has typically involved batch liquid phase systems operated at elevated pressures.[42,77–80] The use of β-Mo_2N to promote ultra-selective continuous gas phase (atmospheric pressure) hydrogenation represents a new direction in the production of industrially important aromatic amines. It must be noted that the β-Mo_2N catalytic system has not been optimized and future work will consider the role of the nitride crystallographic phase/surface area and the catalytic consequences of combining a transition metal (*e.g.* Au or Pd) with the nitride.

3. Experimental

3.1 Mo nitride synthesis

The MoO_3 (99.9995% w/w) precursor was obtained from Alfa Aesar and used as received. Mo nitride synthesis was conducted in a commercial CHEM-BET 3000 (Quantachrome) unit. The precursor (0.150 g MoO_3) was loaded in a U-shaped quartz cell (10 cm × 3.76 mm id) and heated in 15 cm^3 min^{-1} (GHSV = 7×10^3 h^{-1}, Brooks mass flow controlled) 15% v/v N_2/H_2 at 5 K min^{-1} to 933 K. The effluent gas passed through a liquid N_2 trap and changes in composition (consumption/release of H_2 and/or N_2) were monitored by a thermal conductivity detector (TCD) with data acquisition/manipulation using the TPR Win™ software. The reaction was quenched by switching to a He flow (15 cm^3 min^{-1}), the temperature was maintained at 933 K for 3 h and the sample was cooled to room temperature. In order to independently analyze precursor reduction, the thermal treatment of MoO_3 in 15 cm^3 min^{-1} 15% v/v Ar/H_2 at 5 K min^{-1} to 933 K was also monitored. In addition, nitride decomposition was examined by a controlled thermal treatment at 5 K min^{-1} in a flow (60 cm^3 min^{-1}, GHSV = 2×10^4 h^{-1}) of He to 1273 K. Samples for off-line analysis were passivated at room temperature in 1% v/v O_2/He; there was no detectable temperature increase during sample passivation.

3.2 Sample characterisation

Temperature programmed desorption (TPD) and BET surface area measurements were conducted *in situ* in the CHEM-BET unit. After the reduction–nitridation procedure, the sample was thoroughly flushed with Ar for 30 min and a TPD in 65 cm^3 min^{-1} Ar (GHSV = 2×10^4 h^{-1}) to 933 K (at 50 K min^{-1}) was conducted to measure the amount of H_2 released from the nitride. The BET surface area was obtained from analysis in a 30% v/v N_2/He flow with ultra pure N_2 (>99.99%, BOC) as the internal standard. At least two cycles of nitrogen adsorption–desorption in the flow mode were employed using the standard single point BET method. Pore volume measurements were performed using the commercial Micromeritics Flowsorb II 2300 unit. Prior to analysis, the samples were outgassed at 423 K for 1 h and the total pore volume was obtained at a relative N_2 pressure of P/P_0 = 0.95. BET and pore volume measurements were reproducible to within ±5%; the values quoted represent the mean.

Identification of the intermediate and final products was confirmed by XRD, employing a Bruker/Siemens D500 incident X-ray diffractometer using Cu Kα radiation. The samples were scanned at a rate of 0.02° step^{-1} over the range $20° \leq 2\theta \leq 90°$ (scan time = 5 s step^{-1}). Diffractograms were identified by direct comparison with either commercial samples (MoO_3 (Aldrich, 99%) and Mo powder (Aldrich, ≥ 99.9%)) or the JCPDS-ICDD reference standards, *i.e.* MoO_3 (35-609), MoO_2 (32-0671), Mo (42-1120) and β-Mo_2N (25-1368). Diffuse reflectance UV-Vis (DRS UV-Vis) measurements were conducted using a Perkin Elmer Lambda 35 UV-Vis Spectrometer with $BaSO_4$ powder as reference; absorption profiles were calculated from the reflectance data using the Kubelka–Munk function. Analysis by scanning electron microscopy (SEM) was carried out using a Hitachi S2700 field emission SEM unit operated at an accelerating voltage of 10 kV. The sample was deposited on a standard aluminium SEM holder and coated with gold. Elemental (nitrogen) analysis was determined using an Exeter CE-440 Elemental Analyser after sample combustion at *ca.* 1873 K.

3.3 Hydrogenation of *p*-chloronitrobenzene (*p*-CNB)

3.3.1 Catalytic system. The hydrogenation of *p*-CNB (Sigma-Aldrich, purity ≥ 99%) as a solution in ethanol (Sigma-Aldrich ≥ 99%) was carried out under atmospheric pressure at 493 K, *in situ* immediately after β-Mo_2N activation, in a fixed bed vertical glass reactor (l = 450 mm; id = 15 mm). The catalytic reactor and operating conditions to ensure negligible heat/mass transport limitations have been fully described elsewhere[81] but some features, pertinent to this study, are given below. A layer of borosilicate glass beads served as the preheating zone, ensuring that the organic reactant was vaporized and reached reaction temperature before contacting the catalyst. Isothermal conditions (±1 K) were maintained by diluting the catalyst bed with ground glass (75 μm); the ground glass was mixed thoroughly with catalyst before insertion in the reactor. The reaction temperature was continuously monitored using a thermocouple inserted in a thermowell within the catalyst bed. The *p*-CNB reactant was delivered at a fixed calibrated flow rate (F = 0.76 $\mu mol_{p\text{-CNB}}$ min^{-1}) to the reactor *via* a glass/Teflon air-tight syringe and Teflon line using a microprocessor controlled infusion pump (Model 100 kd Scientific). A co-current flow of ultra pure (>99.99%, BOC) H_2 (<1% v/v *p*-CNB in H_2) was maintained at GHSV = 330 min^{-1}; H_2 content was well in excess of the stoichiometric requirement where the flow rate was monitored using a Humonics (Model 520) digital flowmeter. The molar β-Mo_2N to inlet *p*-CNB molar feed rate (n/F) spanned the range 32–128 min. In a series of blank tests, passage of *p*-CNB in a stream of H_2 through the empty reactor did not result in any detectable conversion. The reactor effluent was frozen in a liquid nitrogen trap for subsequent analysis. Carbon balance during the reaction was complete to better than ±4%.

3.3.2 Analytical method and activity/selectivity evaluation. The composition of the reaction/product(s) mixture was determined using a Perkin-Elmer Auto System XL chromatograph equipped with a programmed split/splitless injector and a flame ionization detector, employing a DB-1 capillary column (id = 0.33 mm, length = 30 m, film thickness = 0.20 μm). Data acquisition and manipulation were performed using the TotalChrom Workstation Version 6.1.2 (for Windows) chromatography data system and the overall reactant/product molar fractions (x_i) were obtained using detailed calibrations (not shown). Fractional hydrogenation ($X_{p\text{-CNB}}$) was obtained from

$$X_{p\text{-CNB}} = \frac{[p\text{-CNB}]\text{in} - [p\text{-CNB}]\text{out}}{[p\text{-CNB}]\text{in}} \qquad (3)$$

where selectivity with respect to *p*-chloroaniline (*p*-CAN) is given by

$$S_{p\text{-CAN}}(\%) = \frac{[p\text{-CAN}]\text{out}}{[p\text{-CNB}]\text{in} - [p\text{-CNB}]\text{out}} \times 100 \qquad (4)$$

Repeated reactions with different samples from the same batch of catalysts delivered conversion/selectivity values that were reproducible to within ±7%.

4. Conclusions

We have established that the formation of β-Mo_2N by temperature programmed treatment (to 933 K) of MoO_3 in N_2/H_2 (15% v/v) occurs *via* a kinetically controlled stepwise reduction ($MoO_3 \rightarrow MoO_2 \rightarrow Mo$) and subsequent nitridation ($Mo \rightarrow$ β-Mo_2N). The transformation is non-topotactic with an increase in BET (from 1 to 17 m^2 g^{-1}) and total pore volume (from 2×10^{-3} to 11×10^{-3} cm^3 g^{-1}). Hydrogen TPD measurements have revealed a significant hydrogen content (0.71 μmol m^{-2}) associated with the nitride. We have demonstrated, for the first time, the catalytic action of β-Mo_2N to promote the continuous gas phase hydrogenation of *p*-CNB where *p*-CAN was the sole product, *i.e.* 100% selective in terms of $-NO_2$ group reduction. We have recorded a hydrogenation rate constant (2.0 min^{-1}) for β-Mo_2N that is higher than those achieved with supported transition metals (Au/Al_2O_3, Au/TiO_2 and Pd/Al_2O_3) under comparable reaction conditions. These findings can serve as the basis for the development of Mo_2N materials as new catalysts for the cleaner production of commercially important aromatic amines with multiple applications in the fine chemical industry.

Acknowledgements

The authors are grateful to C. Burnett, R. Blackley and X. Wang for their contribution to this work, which was supported by EPSRC through Grant 0231 110525. EPSRC support for free access to the TEM/SEM facility at the University of St Andrews is also acknowledged as is financial support from the Swiss National Science Foundation.

References

1 V. P. Anitha, S. Vitta and S. Major, *Thin Solid Films*, 1994, **245**, 1–3.
2 K.-I. Machida, A. Nakamoto and G.-Y. Adachi, *Chem. Lett.*, 1993, 1381–1384.
3 V. P. Anitha, A. Bhattacharya, N. G. Patil and S. Major, *Thin Solid Films*, 1993, **236**, 306–310.
4 E. Furimsky, *Appl. Catal., A*, 2003, **240**, 1–28.

5 E. Furimsky and F. E. Massoth, *Catal. Rev. Sci. Eng.*, 2005, **47**, 297–489.
6 S. T. Oyama, *The Chemistry of Transition Metal Carbides and Nitrides*, Blackie Academic, Glasgow, 1996, pp. 14–576.
7 P. Ronsheim, A. Mazza and A. N. Christensen, *Plasma Chem. Plasma Process.*, 1981, **1**, 135–147.
8 L. Volpe and M. Boudart, *J. Solid State Chem.*, 1985, **59**, 332–347.
9 R. Kojima and K.-I. Aika, *Appl. Catal., A*, 2001, **219**, 141–147.
10 R. N. Panda and S. Kaskel, *J. Mater. Sci.*, 2006, **41**, 2465–2470.
11 D. Mckay, J. S. J. Hargreaves and R. F. Howe, *Catal. Lett.*, 2006, **112**, 109–113.
12 R. S. Wise and E. J. Markel, *J. Catal.*, 1994, **145**, 344–355.
13 S. Gong, H. Chen, W. Li and B. Li, *Appl. Catal., A*, 2005, **279**, 257–261.
14 A. Gomathi, A. Simdaresam and C. N. R. Rao, *J. Solid State Chem.*, 2007, **180**, 291–295.
15 X. Zhao and K.-J. Range, *J. Alloys Compd.*, 2000, **296**, 72–74.
16 S. L. Roberson, D. Finello and R. F. Davis, *Thin Solid Films*, 1998, **324**, 30–36.
17 S. Chouzier, P. Afanasiev, M. Vrinat, T. Cseri and M. Roy-Auberger, *J. Solid State Chem.*, 2006, **179**, 3314–3323.
18 P. Afanasiev, *Inorg. Chem.*, 2002, **41**, 5317–5319.
19 R. C. V. Mcgee, S. K. Bej and L. T. Thompson, *Appl. Catal., A*, 2005, **284**, 139–146.
20 C. W. Colling, J.-G. Choi and L. T. Thompson, *J. Catal.*, 1996, **160**, 35–42.
21 G. S. Ranhotra, G. W. Haddix, A. T. Bell and J. A. Reimer, *J. Catal.*, 1987, **108**, 24–39.
22 S. Li, W. B. Kim and J. S. Lee, *Chem. Mater.*, 1998, **10**, 1853–1862.
23 M. Nagai, Y. Goto, A. Miyata, M. Kiyoshi, K. Hada, K. Oshikawa and S. Omi, *J. Catal.*, 1999, **182**, 292–301.
24 S. W. Gong, H. K. Chen, W. Li and B. Q. Li, *Energy Fuels*, 2006, **20**, 1372–1376.
25 K. Inumaru, K. Baba and S. Yamanaka, *Chem. Mater.*, 2005, **17**, 5935–5940.
26 H. J. Lee, J.-G. Choi, C. W. Colling, M. S. Mudholkar and L. T. Thompson, *Appl. Surf. Sci.*, 1995, **89**, 121–130.
27 M. Nagai, *Appl. Catal., A*, 2007, **322**, 178–190.
28 M. Nagai, Y. Goto, A. Irisawa and S. Omi, *J. Catal.*, 2000, **191**, 128–137.
29 M. Nagai, Y. Goto, O. Uchino and S. Omi, *Catal. Today*, 1998, **45**, 335–340.
30 T. Ressler, R. E. Jentoft, J. Wienold, M. M. Günter and O. Timpe, *J. Phys. Chem. B*, 2000, **104**, 6360–6370.
31 T. Ressler, J. Wienold and R. E. Jentoft, *Solid State Ionics*, 2001, **141–142**, 243–251.
32 J. G. Chen, *Chem. Rev.*, 1996, **96**, 1477–1498.
33 L. Volpe and M. Boudart, *J. Solid State Chem.*, 1985, **59**, 348–356.
34 Y. Li, Y. Fan, J. He, B. Xu, H. Yang, J. Miao and Y. Chen, *Chem. Eng. J.*, 2004, **99**, 213–218.
35 D. Liu, Y. Q. Liu, T. Zhou, C. G. Liu and G. H. Que, *Abstr. Pap. Am. Chem. Soc.*, 2003, **226**, U530.
36 Y. Shigehara, *Nippon Kagaku Kaishi*, 1977, 470–474.
37 M. Nagai, Y. Goto, O. Uchino and S. Omi, *Catal. Today*, 1998, **43**, 249–259.
38 M. Nagai, Y. Goto, H. Ishii and S. Omi, *Appl. Catal., A*, 2000, **192**, 189–199.
39 D. Mckay, J. S. J. Hargreaves, J. L. Rico, J. L. Rivera and X.-L. Sun, *J. Solid State Chem.*, 2008, **181**, 325–333.
40 G. Konnecker, A. Boehncke and S. Schmidt, *Fresenius Environ. Bull.*, 2003, **12**, 589–593.
41 P. F. Vogt and J. J. Gerulis, in *Ullmann's Encyclopedia of Industrial Chemistry. "Aromatic Amines"*, Wiley-VCH Verlag GmbH & Co. KGaA, Weinheim, 2005, pp. 2–21.
42 X. D. Wang, M. H. Liang, J. L. Zhang and Y. Wang, *Curr. Org. Chem.*, 2007, **11**, 299–314.
43 P. Delporte, F. Meunier, C. Pham-Huu, P. Vennegues, M. J. Ledoux and J. Guille, *Catal. Today*, 1995, **23**, 251–267.
44 T. Matsuda, Y. Hirata, H. Itoh, H. Sakagami and N. Takahashi, *Microporous Mesoporous Mater.*, 2001, **42**, 337–344.
45 H. Sakagami, Y. Asano, T. Ohno, N. Takahashi, H. Itoh and T. Matsuda, *Appl. Catal., A*, 2006, **297**, 189–197.
46 Y.-J. Zhang, Q. Xin, I. Rodriguez-Ramos and A. Guerrero-Ruiz, *Appl. Catal., A*, 1999, **180**, 237–245.
47 Z. B. Wei, Q. Xin, P. Grange and B. Delmon, *Solid State Ionics*, 1997, **101–103**, 761–767.
48 A. de Lucas Consuegra, P. M. Patterson and M. A. Keane, *Appl. Catal., B*, 2006, **65**, 227–239.
49 T. Ressler, *J. Phys. Chem. B*, 2002, **106**, 7719–7720.
50 E. Lalik, W. I. F. David, P. Barnes and J. F. C. Turner, *J. Phys. Chem. B*, 2001, **105**, 9153–9156.
51 J. Słoczyński, *J. Solid State Chem.*, 1995, **118**, 84–92.
52 G. Xiong, C. Li, Y. Feng, P. Ying, Q. Xin and J. Liu, *J. Catal.*, 1999, **186**, 234–237.
53 H. Aritani, T. Tanaka, T. Funabiki, S. Yoshida, K. Eda, N. Sotani, M. Kudo and S. Hasegawa, *J. Phys. Chem.*, 1996, **100**, 19495–19501.
54 H. Prialiaud, in *Proceeding of the Second International Conference on Chemistry and Uses of Molybdenum*, Climax Molybdenum Co. Ltd., London, 1996, pp. 1–195.
55 K. A. Vikulov, B. N. Shelimov and V. B. Kazansky, *J. Mol. Catal.*, 1991, **65**, 393–402.
56 G. Benítez, J. M. Heras and L. Viscido, *J. Phys.: Condens. Matter*, 1993, **5**, A221–A222.
57 R. Bafrali and A. T. Bell, *Surf. Sci.*, 1992, **278**, 353–363.
58 S. T. Oyama, *Catal. Today*, 1992, **15**, 179–200.
59 J. S. Lee, L. Volpe, F. H. Ribeiro and M. Boudart, *J. Catal.*, 1988, **112**, 44–53.
60 J. S. Lee, S. T. Oyama and M. Boudart, *J. Catal.*, 1987, **106**, 125–133.
61 C. Bouchy, I. Schmidt, J. R. Anderson, C. J. H. Jacobsen, E. G. Derouane and S. B. D. A. Hamid, *J. Mol. Catal. A: Chem.*, 2000, **163**, 283–296.
62 W. V. Schulmeyer and H. M. Ortner, *Int. J. Refract. Met. Hard Mater.*, 2002, **20**, 261–269.
63 A. Guerrero-Ruiz, Q. Xin, Y. J. Zhang, A. Maroto-Valiente and I. Rodriguez-Ramos, *Langmuir*, 1999, **15**, 4927–4929.
64 X. S. Li, Y. X. Chen, Y. J. Zhang, C. X. Ji and Q. Xin, *React. Kinet. Catal. Lett.*, 1996, **58**, 391–396.
65 J.-G. Choi, H. J. Lee and L. T. Thompson, *Appl. Surf. Sci.*, 1994, **78**, 299–307.
66 Z. Wei, Q. Xin, P. Grange and B. Delmon, *J. Catal.*, 1997, **168**, 176–182.
67 X. S. Li, Y. J. Zhang, Q. Xin, C. X. Ji, Y. F. Miao and L. Wang, *React. Kinet. Catal. Lett.*, 1996, **57**, 177–182.
68 Q. Xu, L. Wang, J. R. Chen, X. J. Li and R. X. Li, *Chin. J. Catal.*, 2007, **28**, 579–581.
69 J. Ning, J. Xu, J. Liu, H. Miao, H. Ma, C. Chen, X. Li, L. Zhou and W. Yu, *Catal. Commun.*, 2007, **8**, 1763–1766.
70 B. Zhao, C.-J. Chou and Y.-W. Chen, *Ind. Eng. Chem. Res.*, 2010, **49**, 1669–1676.
71 X. X. Han, J. R. Li and R. X. Zhou, *Chin. Chem. Lett.*, 2009, **20**, 96–98.
72 H. Li, J. Zhang and H. Li, *Catal. Commun.*, 2007, **8**, 2212–2216.
73 M. Mo, L. Han, J. Lv, Y. Zhu, L. Peng, X. Guo and W. Ding, *Chem. Commun.*, 2010, **46**, 2268–2270.
74 F. Cárdenas-Lizana, S. Gómez-Quero and M. A. Keane, *Appl. Catal., A*, 2008, **334**, 199–206.
75 F. Cárdenas-Lizana, S. Gómez-Quero and M. A. Keane, *Catal. Commun.*, 2008, **9**, 475–481.
76 F. Cárdenas-Lizana, S. Gómez-Quero and M. A. Keane, *ChemSusChem*, 2008, **1**, 215–221.
77 H. U. Blaser, H. Steiner and M. Studer, *ChemCatChem*, 2009, **1**, 210–221.
78 Y.-C. Liu and Y.-W. Chen, *Ind. Eng. Chem. Res.*, 2006, **45**, 2973–2980.
79 V. Kratky, M. Kralik, M. Mecarova, M. Stolcova, L. Zalibera and M. Hronec, *Appl. Catal., A*, 2002, **235**, 225–231.
80 B. Coq, A. Tijani, R. Dutartre and F. Figuéras, *J. Mol. Catal.*, 1993, **79**, 253–264.
81 G. Tavoularis and M. A. Keane, *J. Chem. Technol. Biotechnol.*, 1999, **74**, 60–70.